

We are IntechOpen, the world's leading publisher of Open Access books Built by scientists, for scientists

6,900

Open access books available

186,000

International authors and editors

200M

Downloads

Our authors are among the

154

Countries delivered to

TOP 1%

most cited scientists

12.2%

Contributors from top 500 universities



WEB OF SCIENCE™

Selection of our books indexed in the Book Citation Index
in Web of Science™ Core Collection (BKCI)

Interested in publishing with us?
Contact book.department@intechopen.com

Numbers displayed above are based on latest data collected.
For more information visit www.intechopen.com



Chapter

Metal 3D-Printing of Waveguide Components and Antennas: Guidelines and New Perspectives

*María García-Vigueras, Lucas Polo-Lopez,
Charalampos Stoumpos, Aurélie Dorlé, Carlos Molero
and Raphaël Gillard*

Abstract

This chapter intends to show the strong potential brought by metal 3D-printing to the field of waveguide components and antennas. General co-design guidelines are firstly provided. These guidelines enable to benefit from the advantages associated to metal 3D-printing. The implementation of filters and ortho-mode transducers is considered, together with horns and slotted antennas. Finally, multifunctional periodic structures benefiting from metal 3D-printing are discussed.

Keywords: 3D-printing, additive manufacturing, selective laser melting, ortho-mode transducers, filters, polarizers, leaky-wave antennas

1. Introduction

3D-printing has made a profound impact in the development of radio-frequency (RF) devices in the past decade. Initially, this manufacturing technique represented an opportunity to implement new ideas as well as to enjoy fast, cost-effective, and monolithic prototyping [1–8]. However, non-negligible constraints were found in the first attempts to 3D-print RF components. Such constraints were associated, for example, to surfaces rough finish, the appearance of undesired supports, and the need for electroless plating. Neither the resulting manufacturing tolerances were optimal, nor the quality of the printed pieces. With time, as a result of collective efforts, it has been understood that the full benefit of this technique (i.e., short lead time, low cost, single piece prototyping, and high RF quality) implies a change of mindset in RF design [9–13]. As a result, today we are witnessing the most disruptive impact of 3D-printing: the challenge of the bounds of our creativity and the need for new co-design guidelines.

3D-printing consists in the layer-by-layer additive manufacturing (AM) of objects. Different materials can be employed to build the piece. For example, plastic polymers can be used to build objects through stereolithography (SLA) [6, 7]. The case of the present chapter considers selective laser melting (SLM), which allows to use metal alloys

as the building material [10, 14–16]. Examples found in the literature include aluminum (which is the most extended one, AlSi10Mg), titanium, stainless steel, or Invar. This option is the preferred one when dealing with aerospace applications. The main associated advantage is that it directly leads to a body that can easily meet the stringent mechanical and thermal conditions associated to space or other harsh environments. Additionally, metallic 3D-printed parts are compatible with high-power handling, specially if they are monolithic, as passive inter-modulation issues are minimized.

The main disadvantage of metal 3D-printing is the surface finish of the 3D-printed part. The resulting surface roughness is larger than what is normally obtained with conventional manufacturing techniques, which results in higher insertion losses. Consequently, 3D-printed parts might exhibit higher loss than the counterpart produced with CNC milling. For that reason, postprocessing and additional surface metallization techniques are currently being developed in order to improve the conductivity of a metal part [17]. The effective conductivity of a 3D-printed waveguide depends on many aspects such as the frequency of operation, the chosen printing direction, or the shape; however, an average value for a raw (not metallized) finish is 0.5×10^7 S/m. With treatments, values of up to 3×10^7 S/m can be achieved. This is still less than the ideal conductivity of aluminum; however, it has been noticed that the devices do give competitive loss thanks to the avoidance of assembly, which might create leakage or reflections.

Current metal 3D-printers offer printing volumes that range from $250 \text{ mm} \times 250 \text{ mm} \times 250 \text{ mm}$ [18] to $400 \text{ mm} \times 400 \text{ mm} \times 400 \text{ mm}$ [19], which are well suited for devices operating from X-band. At the time this chapter is being written, one can find stories in the media where the main space primes have announced the use of 3D printing in their future high-throughput satellites [20–22]. On the other hand, in 2021, a European Cooperation for Space Standardization (ECSS) standard with requirements for processing and quality assurance of powder bed fusion technologies for space applications has been issued [23]. All this together proves that the space industry recognizes the maturity of metal 3D-printing and accepts its use for present and future systems.

The authors of this chapter have been involved in several R&D projects related to 3D-printing of RF components and antennas. Such projects have been mainly conducted in France, at the laboratory IETR (Institut d'Electronique et des Technologies du numÉrique), and they have been funded by the European Union, the European Space Agency (ESA), the Centre National d'Etudes Spatiales (CNES), and the Region of Brittany. Such projects have allowed the conception of general design guidelines for successful SLM prototyping, which are next provided in Section 2. In the following sections, advanced 3D-printed parts are described. Section 3 includes the implementation of waveguide components, such as filters and ortho-mode transducers. Section 4 considers the development of horns and slotted antennas. The case of periodic structures implementing frequency selective filtering and polarization conversion is considered in Section 5. Finally, conclusions are drawn in Section 6.

2. General design guidelines

A general belief when approaching 3D-printing is that any RF geometry can be fabricated. Still, while there is significant freedom and possibility to fabricate complex shapes, there are also a series of rules and guidelines that allow to obtain optimal results out of 3D-printing.

The set of guidelines is indeed very broad, since it goes from the initial RF design of geometry to the type of machine parameters used to fabricate the part. This section will only cover the ones concerning the RF designer, since the rest will change depending on many considerations, ranging from the type of machine to productivity. In any case, and as it will be demonstrated in this chapter (which contains many examples from different authors and therefore different manufacturers), the basic RF guidelines are enough to produce very good performance regardless of the 3D printer, alloy, or manufacturer.

Concerning RF design, the most basic consideration when 3D printing RF devices is the orientation that the piece will have in the 3D printer. Such orientation determines the manufacturing tolerances, the degree of symmetry of the printed component, the eventual need of supports if the printer finds surfaces that are hanging, and the number of parts that one can print in the same platform. In order to attain both high precision and high symmetry, the piece should be oriented in a way that either the main waveguide propagation axis is parallel to the building direction (vertical printing) or the main waveguide propagation axis is perpendicular to the building direction (horizontal printing).

The remaining of the subsection discusses the basic guidelines that a designer may follow to adapt a waveguide device to vertical or horizontal printing.

2.1 Overhanging faces

Overhanging faces are those that are perpendicular to the printing direction and facing down, as illustrated in **Figure 1(a)**. As part of the design process, such overhanging faces should be modified, since they can suffer strong deformation or even collapse if they are too big. The recommended design practice is to chamfer or tilt the face with an angle of 45° or larger. As it will be shown later, this technique can be applied to corrugations, irises, cavities, posts, etc.

2.2 Wall thickness

In certain microwave devices, thin walls are needed as part of the RF design (e.g., septums in orthomode transducers, irises in filters, inner walls in power dividers, etc). To the best knowledge of these authors, the lowest wall thickness that can be 3D-printed nowadays with a good reliability is 0.5 mm. In certain

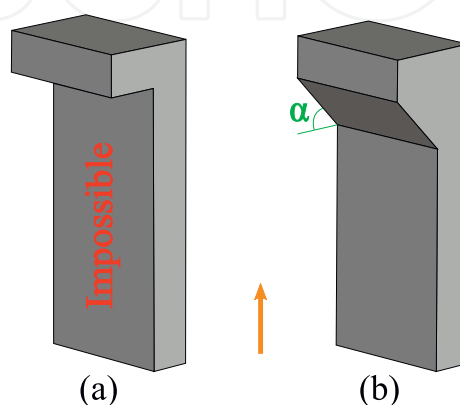


Figure 1. Nonfeasible overhanging face (a) and feasible inclined overhanging face (b). The orange arrow indicates the printing direction.

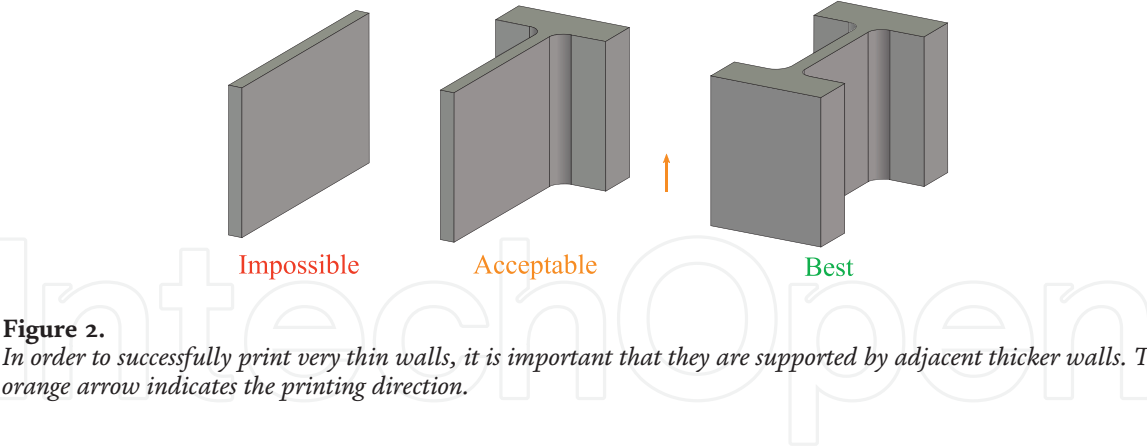


Figure 2.
In order to successfully print very thin walls, it is important that they are supported by adjacent thicker walls. The orange arrow indicates the printing direction.

occasions, it can be possible to achieve thicknesses of 0.3 mm, although only for very short walls and supported by thicker adjacent walls, as illustrated in **Figure 2**.

2.3 Height

When creating elongated structures such as posts, it is important to take into account that their height should not be greater than five times the diameter of the base. If this requirement is not satisfied, the post can suffer deformations. In the case that it would be necessary to use a feature that does not satisfy the previous criteria, the recommendation is to use a truncated post (or a prism whose base is larger than the top face), as it is indicated in **Figure 3**.

2.4 Rounded edges

Rounding of the edges of the structure is welcome for 3D-printing. The recommended rounding radius is at least 0.3 mm (although the larger, the better). The reason for this recommendation is the avoidance of local overheating when printing a certain edge, which can result in deformations of the structure [24].

2.5 De-powdering

The “de-powdering” is the activity where all the unmelted powder is removed from the fabricated part. The RF designer should conceive the device avoiding highly concave cavities (those whose only opening is very small when compared with the size of the cavity) as well as minimizing (if possible) the presence of siphon waveguide sections.

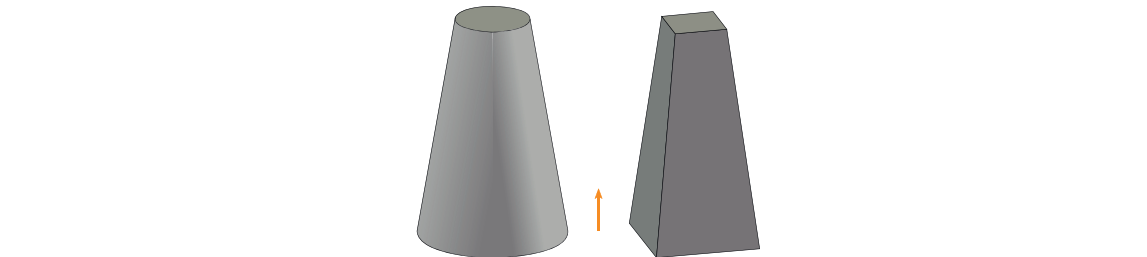


Figure 3.
Different approaches to increase the stability of elongated structures. The orange arrow indicates the printing direction.

2.6 Machining of waveguide flanges

Finally, a highly recommended RF practice is the reworking of the flanges using CNC milling in order to ensure a perfect connection with the rest of the devices.

3. Waveguide components

3.1 Filters

Waveguide filters are devices used to select and/or reject signals in an RF chain. The implementation in waveguide technology ensures low losses and high-power handling, while its main disadvantages are the associated mass and the volume. In contrast to other waveguide devices listed in this chapter, filters are, in general, rather sensitive to the manufacturing tolerances. As a result, the use of the previous design guidelines is even more relevant in the present case.

In the domain of metallic 3D-printed filters, it is possible to find multiple articles where AM is used to enable the prototyping of complex geometries [25]. In such examples, the printing direction has not been specifically considered as part of the design process, which is the purpose here. In the following, two examples are illustrated that are based either on vertical and horizontal printing (associated respectively to waveguides whose propagation axis is either parallel or perpendicular to the printing direction) (**Figure 4**).

In the case of vertical printing, traditional filter topologies shall be adapted by tilting all their down facing parts so that they become self supporting. A first example is proposed in [15], where $\lambda/4$ rejection stubs are tilted. The authors of such paper present prototypes in Ku/K-band that have been fabricated using different metal alloys. All the filters present high rejection (50 dB) and low insertion losses (from 1 to 0.1 dB, depending on the type of surface finish). Another example can be seen in [11], where a bandpass filter with titled irises is presented. The design in the article is a 11-pole filter operating from 17.3 to 20.2 GHz. The two fabricated filters exhibit a bandwidth slightly narrower than the simulated one. An interesting result is the great similarity between the two prototypes, which have been produced using different processes with the same alloy. The latter is a confirmation of what was stated in Section 1: using guidelines for 3D-printing enables robust filter designs. A third example can be found in [16], where a corrugated filter with chamfered corrugations is presented. The filter also operates in the Ka-band (17.7–20.2 GHz) and provides all-mode rejection up to 43 GHz. This work also provides a comparison between raw

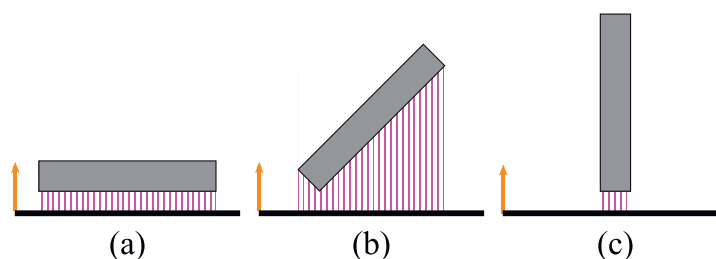


Figure 4. Different orientations of a filter (gray) on the building platform (black) and the required supports (magenta) for each of them. The orange arrow indicates the printing direction.

(not metallized) and metallized finish, where the associated ohmic losses are 0.35 and 0.25 dB, respectively.

Interestingly, there are also filter examples that by default (without requiring dedicated design guidelines) are compatible with vertical printing such as the filters based on spherical or quasi-spherical resonators. In [26], a dual-mode filter at 8.25 GHz implemented with spherical cavities (which can support two modes) and compatible with vertical printing is presented. Dual-mode filters are known for being very sensitive and often require tuning screws; however, the 3D-printed filter in the article achieves a performance very close to simulation without the need of tuning screws, which is another demonstration of the suitability of vertical printing for the production of waveguide filters.

Ridge waveguide evanescent mode filters can also be adapted to vertical printing. These filters are based on the cascading of ridge and hollow waveguide sections of the same width and height. By chamfering the ridges as in **Figure 5**, the filter becomes vertically printable, as demonstrated in [12].

Figure 6 shows the measured and simulated performance of one filter of this kind. Two identical samples of the filter have been manufactured in order to verify its repeatability. As it can be appreciated, the results of both prototypes show excellent agreement between them and also with the simulation. The insertion losses (0.3 dB) are in agreement with the expected value for a nonmetallized component.

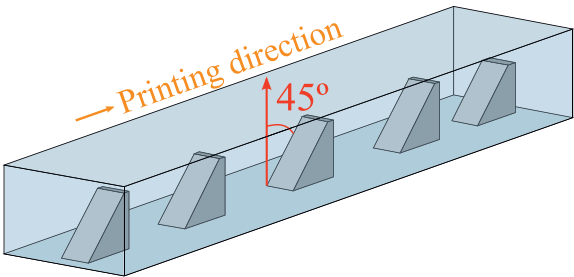


Figure 5. Representation of an evanescent mode ridge waveguide filter designed to be vertically printable. The ridges have been chamfered with a 45° angle so that they become self-supporting.

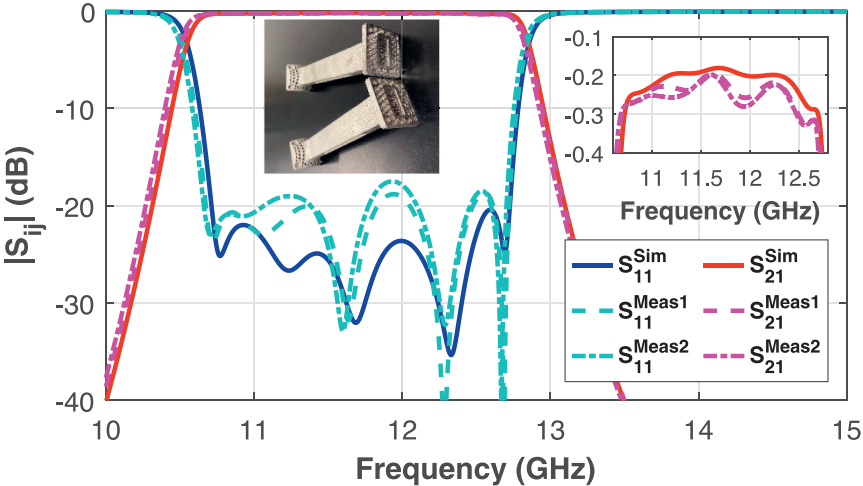


Figure 6. Simulated and measured scattering parameters of an evanescent mode filter with chamfered ridges. Two copies of the prototype have been manufactured in order to assess the repeatability. These figures are shown here for the first time.

An example of horizontal printing can be found in [17]. In that work, the authors report a combline filter where the cavities have triangular cross section. When 3D-printing this filter, the combline post grows from the base of the triangle, while the other two sides of the triangle (with an angle with respect to the base larger than 45°) converge vertically until they find each other, thus closing the cavity.

Another common practice in 3D-printed filters is the introduction of features in order to improve the performance (quality factor enhancement, extension of spurious-free band, etc). One example can be seen in [11], where a dimple has been created at the center of each cavity. Such feature has negligible impact on the insertion loss but pushes up the repeat band.

3.2 Orthomode transducers and polarizers

Orthomode transducers (OMTs) are commonly used to separate or combine two orthogonally polarized signals from or into the same waveguide. OMTs typically operate in linear polarization, and its key figures of merit relate to the isolation between the rectangular ports and cross-polarization discrimination (XPD) between the signals in the dual-polarized port. Septum polarizers are a type of OMT that also converts from linear to circular polarization and vice versa.

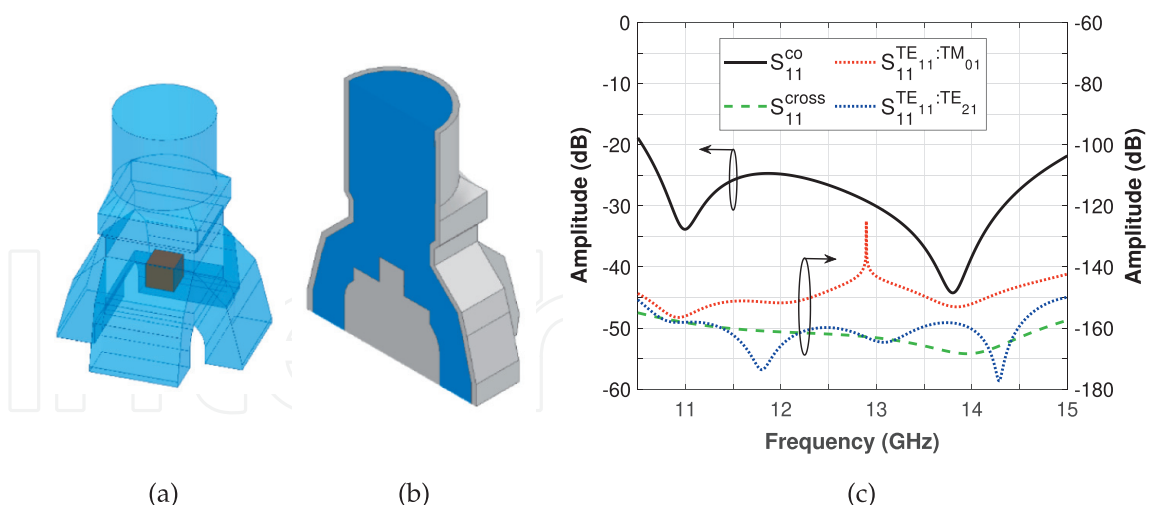
The isolation and XPD of an OMT depend on the structural symmetry of the component [27]. Potential asymmetries as consequence of fabrication will produce unwanted coupling between signals that are supposed to be orthogonal. As it has already been mentioned, the structural symmetry is better assured when the components are printed in vertical direction, hence the importance of the design guidelines for OMTs.

It is worth starting by the contribution in [9], which reports both side-arm OMT and septum polarizer in the Ka-band that are adapted to vertical printing. While the septum polarizer does not require much effort for 3D-printing, the side-arm OMT has been redesigned in a way that the “side” waveguide presents the top faces tilted in order to be self-supporting. Several E-plane matching steps are required to obtain optimal matching. Both devices are single-band and exhibit measured isolation and XPD in excess of 30 dB.

In [28], the authors present a Ka-band dual-band Bøifot OMT also adapted for vertical printing. The back face of the inner septum in charge of splitting/combining the polarizations has been chamfered according to the printing direction. It exhibits isolation and XPD greater than 40 and 30 dB, respectively, over 18.6–20.2 GHz and 28–30 GHz.

Interestingly, and despite being one of the most commonly used OMTs, there is no work in the literature with vertically printable turnstile OMTs. Two design concepts are discussed here for the first time. The first concept of such a design is depicted in **Figure 7(a)-(b)**, which shows the CAD model of the five-port turnstile junction. The main difference with respect to conventional designs is the four rectangular single-polarized waveguides, which are tilted to the junction axis so that they do not show unsupported faces. As **Figure 7(c)** also proves, the performance of the modified junction (reflection coefficient level lower than -25 dB is achieved for the full Ku-band SATCOM bandwidth, 10.7–14.8 GHz) does not show any limitation despite the modification.

The second design concept, in **Figure 8**, exploits the use of truncated cones for the realization of the turnstile post. One design approach when the bandwidth of OMT gets larger is the use of multistep posts [29]. As it has been discussed earlier, this type of

**Figure 7.**

First concept of a Ku-band (10.7–14.8 GHz) self-supporting turnstile-based OMT in vertical full-metal 3D-printing to avoid overhanging parts during the print process: (a) perspective view of the RF layout of the five-port junction (the transparent blue part is vacuum and the brown part is the metallic turnstile post), (b) transparent vertically cut view of the mechanical layout of the five-port junction (the blue part is vacuum and the gray part is metal), and (c) simulation results (port 1 refers to the common circular port).

feature is not well suited for vertical printing, hence truncated cones are used to design components with increased bandwidth (17.7–31 GHz, with matching better than -20 dB in the uplink and downlink SATCOM bands). In this case, the OMT is terminated using E-plane power combiners designed in hexagonal waveguide. This second design has been fabricated and measured, and the results are depicted in **Figure 8(c)**. The measured reflection coefficients for both polarizations remain below -20 dB over the bands of interest (18–21.2 GHz and 27.5–31 GHz), while they also show a good agreement with simulations (not shown for clarity). The cross-polarized transmission coefficients and the rectangular ports present coupling levels below -35 dB and -45 dB, respectively. The transmission coefficients are better than 0.5 dB (it must be noticed that the test setup requires extra waveguides in order to match the device nonstandard ports to standard ports and therefore the measured losses are higher than the ones of the component itself).

To complete the section, it is worth highlighting an interesting recent trend consisting in the combination of several OMTs in a single device to create a N-way OMT, possibility, which is enabled by the design freedom inherent to 3D-printing. The work in [30, 31] presents a four-way OMT-power divider, which is built as an array of 2×2 asymmetric side-arm OMTs in a tight square grid (around $1.25\lambda_0$) fed by two distributed 1×4 single polarized power dividers. The component was conceived without overhangs so it can be vertically printed. The measured prototypes feature isolation and XPD better than 40 dB.

4. Antennas

4.1 Horns

Horn antennas are widely used in various microwave and millimeter-wave applications, from feeds for reflectors to phased arrays or in antenna measurements. Such

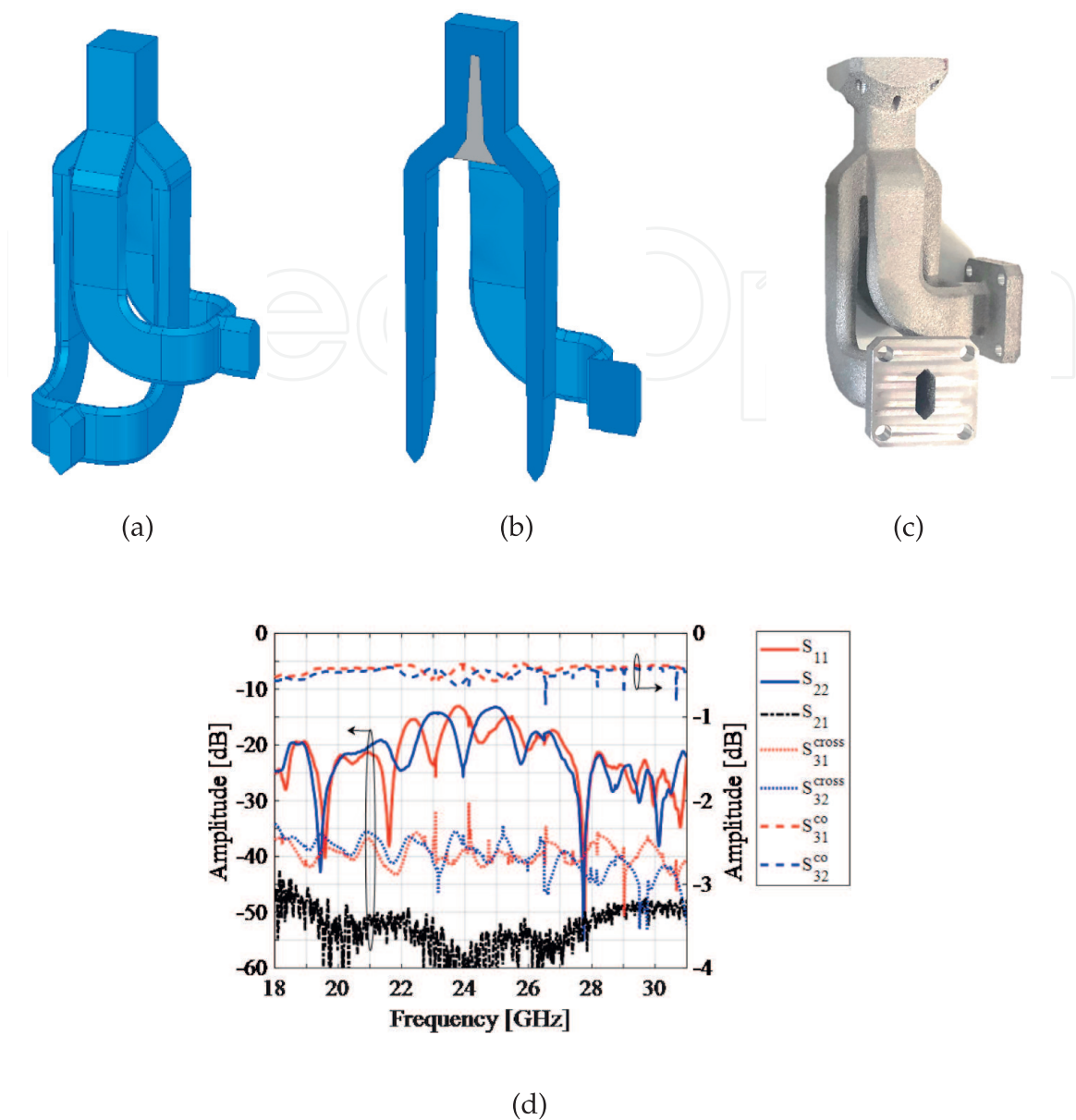


Figure 8. Second concept of a dual-Ka-band (18–22 GHz and 27–31 GHz) self-supporting turnstile-based OMT in vertical full-metal 3D-printing to avoid overhanging parts during the print process: (a) perspective view of the total OMT's RF layout (the blue part is vacuum), (b) vertically cut view of the total OMT's RF layout (the blue part is vacuum and the gray part is the metallic turnstile post), (c) photograph of the printed prototype, and (d) measurement results. These results are shown here for the first time and they are courtesy of SWISSto12.

wide range of applicability is attributed to their robust RF performance such as medium or high gain, wide bandwidth, high XPD, and low losses.

As far as 3D-printing is concerned, horn antennas can be separated into two fundamental categories: (1) smooth-walled flared horns (this category includes different type of profiles such as pyramidal, spline, or Potter) [9, 31–36]; and (2) axially corrugated horns [37–39]. Regardless of the horn type, the printing direction shall be vertical in order to preserve the symmetries of the structure.

Stepped smooth-walled horns are discussed in [33], which presents designs operating in Ku-, Ku/K-, and Q/V-band. The three horns are printed vertically; consequently, the measured and simulated results of all antennas exhibit a good agreement. Particularly interesting is the results of the Q/V-band device, where a XPD better than -28 dB over the whole frequency band has been obtained experimentally.

Spline horns (smooth-wall horns whose flare follows a spline function) are presented in [32, 35]. These industrial works coincide in presenting Ku-band horns that are later integrated in a horn cluster (monolithic device including several horns as well as their corresponding feed devices). Moving on to horn clusters for the production of large horn arrays enables strong mass and cost reduction: on the one hand, the total number of parts (from bolts to mechanical brackets to the RF device) is drastically reduced, which has an impact on both the mass and the cost (dealing with all these parts requires an associated effort). On the other hand, the integration of a cluster is much simpler and faster, which reduces the overall program cost. This trend, which is enabled by 3D-printing, seems to be the future of Geostationary (GEO) telecommunication satellites [40].

In [34], a ridged horn antenna with multistep flare is presented. It is worth highlighting the high frequency achieved by this design (110 GHz), which is another proof of the very high performance that one could achieve when following the design guidelines. Moreover, extra features (corrugations) are added around the horn aperture in order for the horn to maintain high RF performance over a very wide bandwidth (45–110 GHz). This is another example of exploiting the design freedom of 3D-printing to improve the RF performance without increasing the manufacturing complexity.

Similarly, the work in [36] exploits the design freedom to consider perforations on the metallic walls of the horn to reduce mass without affecting the performance. The considered perforated gaps are smaller than $\lambda_0/15$ and hence opaque for the electric field. The experimental results demonstrate the suitability of such practice, which leads to a mass reduction in the order of up to two-thirds with respect to a horn.

To complete the survey of smooth-walled horns, it is also worth highlighting the work in [31], which presents a very high efficiency horn operating in the downlink Ku-band (10.7–12.75 GHz). The device, which is called quad-furcated profiled horn antenna, consists of four asymmetric small horns forming a 2×2 array that feeds a square waveguide aperture. The device also includes the feed network. All features in the component are compatible with vertical printing. The measured performance (S-parameters and radiation patterns) shows excellent agreement with the simulated one. This approach, which holds potential to use the power on board the GEO satellite more efficiently than other horn designs, can only be conceived with use of 3D-printing.

The design and fabrication of axially corrugated horns are presented in [37–39]. In particular, the accuracy and repeatability of 3D-printed choke horns at X/Ku band are investigated in [38]. Fifteen antennas were manufactured and tested, showing a coherent agreement between simulations and measurements in terms of matching, radiation efficiency, and radiation patterns. An axially corrugated horn covering the full Ka-band (26.5–40 GHz) is presented in [39], whose measured radiation patterns show good beam symmetry and XPD better than 29 dB. Reference [37] shows a choke horn that acts as feed in a transmitarray for cubesat applications. The antenna works in the range 23–26 GHz and is fabricated together with a septum polarizer.

Finally, to the best knowledge of these authors, there is no work reporting conventional corrugated horns where the corrugations are adapted to vertical printing. Nevertheless, the techniques described in [15] or [16] should be applicable to horns too.

4.2 Slotted antennas

Slotted waveguide antennas (SWAs) are attractive solutions for millimeter-wave applications because they enable high gain with a simple and flat beamforming network architecture. SWAs consist of a waveguide where one of the walls is periodically

perforated with radiating slots. Generally speaking, SWAs can be grouped into two categories: resonant SWAs and non-resonant SWAs.

Resonant SWAs, which produce broadside radiation, use $\lambda_g/2$ inter-element spacing between the successive slots (where $\lambda_g/2$ is the wavelength in the waveguide) as well as they have a shorted termination. On the contrary, non-resonant SWAs do not produce broadside radiation and have inter-slot spacing that is different from $\lambda_g/2$ as well as a matched termination.

Regardless of the antenna type, SWAs exhibit a narrow bandwidth, which depends on several geometrical parameters, such as slot dimensions and shape, metal thickness, and inter-slot distance [41]. Nevertheless, this bandwidth can be widened using well-known design approaches such as separation of the array into several sub-arrays [42], use of ridge-waveguide [43], use of elliptical slots and direct coaxial feeding [44], as well as coupled-slot and differential feeding mechanisms [45].

Although the printing rules described in Section 1 apply also for slotted antennas, most of the works available in the literature report printing orientations of 45° with respect to broadside direction. Such works are not sensitive to the symmetry of the piece, therefore such orientation gives satisfactory results.

In [3], an 8x8-element resonant SWA in Ku-band with a corporate beamforming network is presented. Interestingly, this work also reports a counterpart based on subtractive manufacturing of several parts that are later assembled. The comparison between the two antennas shows that the 3D-printed antenna has a gain that is 1–1.5 dB larger than the traditionally manufactured antenna. In the latter, gaps and alignment errors between metal layers cause leakages and reflections, which are critical enough to eventually degrade the antenna performance. The article also discusses the fabrication orientation and the fabrication supports, which are the main disadvantages of this manufacturing approach. The same authors expand their work on SWAs in [46], which also operates in Ku-band but is much larger (16×16) as well as implements a monopulse comparator. As in the previous work, and despite the higher complexity and size of this component, the measured results show great similarity with the simulation, which validates the printing direction orientation.

An assessment on planar and conformal 1D and 2D resonant SWAs is presented in [47]. Several orientations and machine settings were studied to obtain consistent parts with high detail resolution and quality. The study includes also investigation of manufacturing defects and surface roughness of the components.

Concerning non-resonant SWAs, it is worth highlighting the leaky-wave antennas [48] reported in [49–51], operating in different frequencies ranging from K- to V-band. Despite these publications involving plastic printing, the antenna in [50] was later used to build an array in metal. The novelty in these works is that additive manufacturing enables dual-polarization radiation from a single leaky-wave aperture and to consider an OMT printed together with the antenna. Moreover, inner ridges with modulated geometry have been considered inside the leaky waveguide, which enable low side-lobe level for the two linear polarizations. The array shown in **Figure 9** was conceived as an extension of the previous work and is here presented for the first time. The beamforming network is folded toward the back side of the antenna, and the whole is printed in a single piece. A summary of the measured performance is presented in **Figure 10**. A very good agreement with simulation is obtained for patterns and directivity over the operating bandwidth, demonstrating again the suitability of 3D-printing for SWA. The backward lobe in the pattern is produced by the short-circuit created at the end of the antenna. Such beam could be avoided by using a matched load.

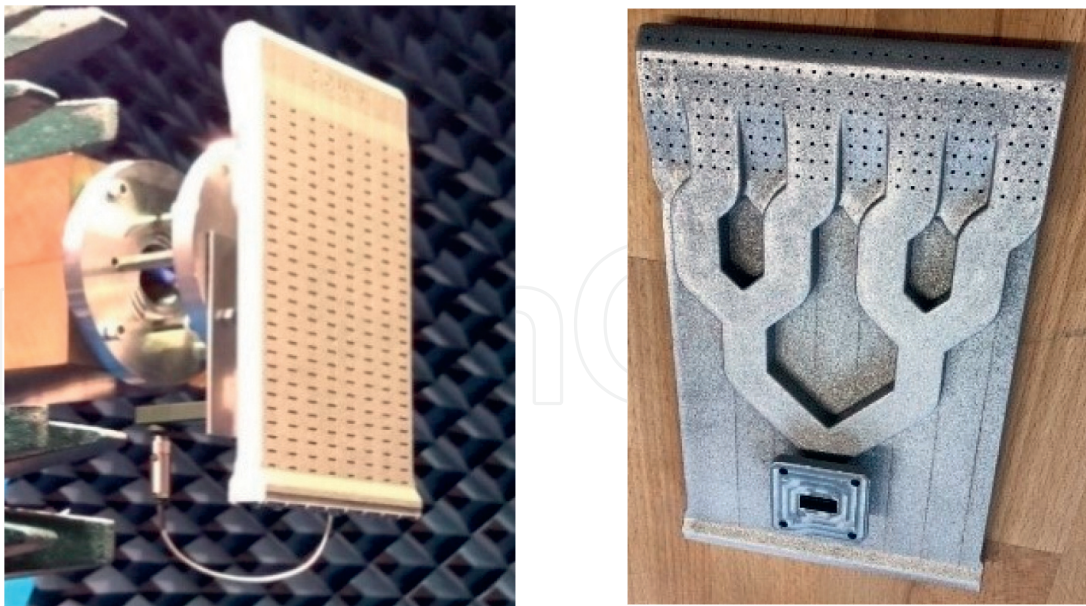


Figure 9.
SLM printed compact ridged linearly polarized 2D leaky-wave array with folded beam-forming network.

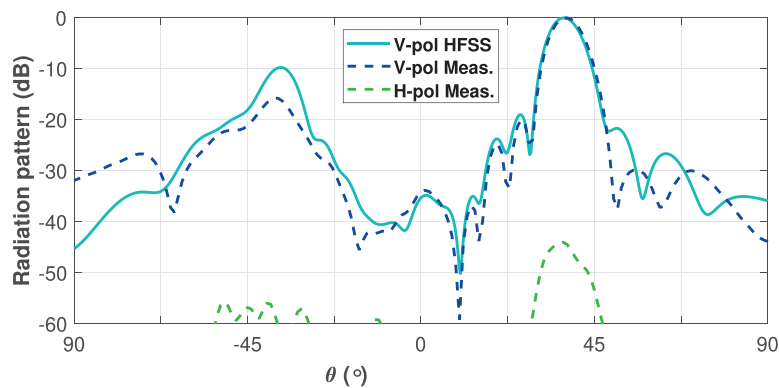


Figure 10.
E-plane pattern (dBi) of the SLM shorted array at 20 GHz.

Finally, an evolution of the previous works is presented in [52], which reports a fully metallic leaky-wave antenna radiating in circular polarization. One of the main original contributions of such work is related to the further plating of the SLM antenna. Such posttreatment step allows to reduce surface roughness and to improve the antenna radiation efficiency (around 10% improvement), as it can be seen in **Figure 11**.

5. Versatile periodic and quasi-periodic structures

Screens based on the periodic and quasi-periodic arrangement of unit cells are widely used nowadays due to their capability to alleviate the complexity of RF feeds in terms of operation frequency, beam shape, polarization, impedance matching, and focusing of the beam, among others. The screens that are currently employed in RF systems are mostly implemented in printed-circuit board (PCB) technology [53]. In order to allow for the wide industrialization of full-metal solutions, a change of paradigm is needed, both in RF design and in manufacturing.

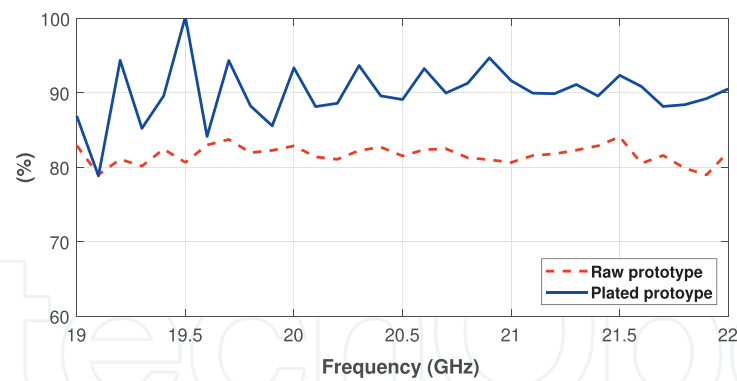


Figure 11. Radiation efficiency (%) for both the raw and posttreated SLM circularly-polarized SWA in [52].

On the one hand, getting rid of the dielectric materials in the design of periodic surfaces is not evident, and it brings significant limitations to the RF designer. A monolithic architecture is needed that allows to be manufactured in metal without supports. A 3D topology is expected to be the future choice in this context, since it allows for greater design freedom. Additionally it is needed to count on a cell with sub-wavelength periodicity in order to avoid the appearance of grating lobes. Such an objective is easily attained in PCB solutions due to the miniaturization brought by the dielectric permittivity. However, when full-metal solutions are made sub-wavelength, they become very reactive and thus, tend to present a high reflection to the impinging waves. As a conclusion, a trade-off seems to appear in full-metal unit cells between the periodicity and the reflectivity when operating in transmission.

On the other hand, 3D-printing appears in this context as the technology for that enables greatest design freedom. However, the guidelines for metal 3D-printing have to be considered early in the phases of RF design.

Most of the metallic 3D screens that can be found in the literature are implemented through plastic 3D-printing and postprocessing of the piece with additional metal coating. This method can be effective, but it is very sensitive to such coating process. In addition, the effective conductivity of some commercial metallic inks or sprays can sometimes be lower than expected, contributing to a strong rise of ohmic losses. Some examples can be mentioned in this category. Negative-refractive index lenses have been reported in [54], metallic reflectarrays in [55, 56], and pass-band frequency selective surfaces in [57–59].

SLM has been applied for the design of periodic distributions of 3D helices, which would be very difficult to implement with other manufacturing techniques. Arrays of helices create artificial anisotropic panels that can be used for the design of polarization converters [60, 61]. Furthermore, additional dielectric supports were necessary to gain robustness. This fact dilutes the term “fully metallic” and strengthens the complexity of conceiving full-metal and self-supporting surfaces.

A metallic transmittarray has been reported in [62]. Its behavior is based on the excitation of a dispersive mode in a waveguide-shape unit cell. Solutions based on waveguide unit cells have also been proposed for the design of dual-band polarizers that provide orthogonal sense of polarization rotation in each band [63]. Such structure was based on highly subwavelength cells, in order to avoid excitation of grating lobes. Unfortunately, the previous designs were not driven by any co-design guideline. The previous geometries were conceived basing on classical RF guidelines, and they did not allow to be implemented in additive manufacturing.

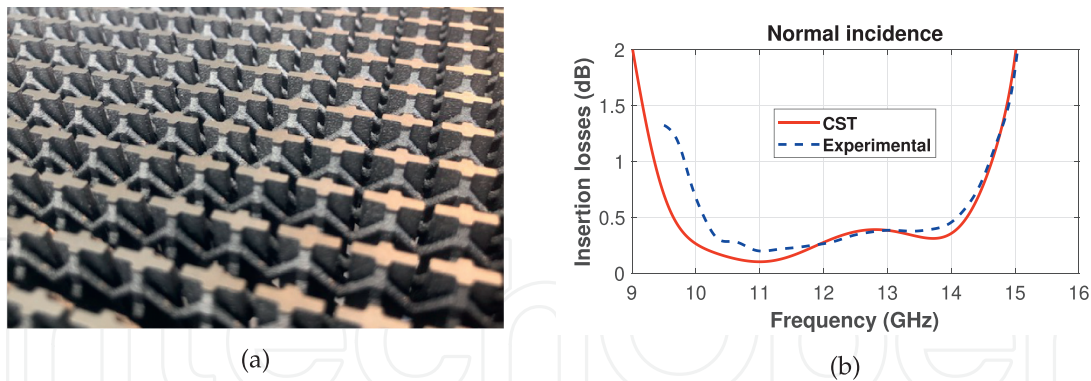


Figure 12.
3D-printed polarizing screen: (a) photograph of the prototype, (b) insertion losses (measured and simulated).

More recently, a topology of 3D unit cell has been proposed, which is specially suited to be 3D-printed [10, 64]. To the best knowledge of these authors, this is the first proof of concept in the literature of a periodic structure that is self-supporting and monolithically 3D-printed in metal. Such a screen is designed to achieve polarization conversion in a broad frequency band. The screen is low dispersive thanks to the excitation of transverse electromagnetic modes within the unit cell. A co-design approach based on the design guidelines detailed in Section 1 was followed in this case, thus enabling accurate prototyping. As an interesting example, bent metallic columns (inclined 45° with respect to the printing direction) were considered. The concept is illustrated in **Figure 12(a)**, which shows a Ku-band prototype printed in aluminum. The bent columns can be easily visualized in the photograph. The insertion losses are plotted in **Figure 12(b)**, they remain below 0.5 dB in the whole frequency band. These results are shown here for the first time. The axial-ratio level is quite similar to that reported in [10]. The architecture depicted in the picture can be adapted for other dual-polarization functionalities beyond polarization-conversion [64].

6. Conclusions

This chapter provides a wide overview of metal 3D-printing applied to the design of various types of waveguide components, antennas, and versatile periodic structures. It can be concluded that the use of 3D-printing can bring multiple relevant advantages when a set of guidelines are followed from early steps in the conception of the RF devices. This chapter opens wide perspectives for the conception of new disruptive RF devices through 3D-printing. The future trend concerns the development of 3D topologies with enhanced performance, complex functionality, and many degrees of freedom. New synergies are expected in RF design combined with powerful optimization techniques that are capable of managing such amount of geometrical parameters. Finally, new theoretical models are expected to appear, providing valuable physical insight on the phenomena underlying the operation of this new 3D structures.

Acknowledgements

This publication is supported by the European Union through the European Regional Development Fund (ERDF) and by the french region of Brittany, Ministry of

Higher Education and Research, Rennes Métropole and Conseil Départemental 35, through the CPER Project SOPHIE/STIC & Ondes, and also by the region of Brittany under grant SAD volet. Additional funding comes from the European Space Agency, the Centre National d'Études Spatiales, the companies Thales Alenia Space, Thales Group, and SWISSto12.

Conflict of interest

The authors declare no conflict of interest.

Author details

María García-Vigueras^{1*}, Lucas Polo-Lopez¹, Charalampos Stoumpos¹, Aurélie Dorlé², Carlos Molero³ and Raphaël Gillard¹


1 Institut d'Electronique et des Technologies du numéRique (IETR), INSA Rennes, Rennes, France

2 ONERA – The French Aerospace Lab, Toulouse, France

3 Universidad de Granada, Granada, Spain

*Address all correspondence to: maria.garcia-vigueras@insa-rennes.fr

IntechOpen

© 2022 The Author(s). Licensee IntechOpen. This chapter is distributed under the terms of the Creative Commons Attribution License (<http://creativecommons.org/licenses/by/3.0>), which permits unrestricted use, distribution, and reproduction in any medium, provided the original work is properly cited. 

References

- [1] Sorrentino R, Peverini OA. Additive manufacturing: A key enabling technology for next-generation microwave and millimeter-wave systems [point of view]. *Proceedings of the IEEE*. 2016;**104**(7):1362-1366
- [2] Guo C, Shang X, Lancaster MJ, Xu J. A 3-d printed lightweight x-band waveguide filter based on spherical resonators. *IEEE Microwave and Wireless Components Letters*. 2015; **25**(7):442-444
- [3] Huang G-L, Zhou S-G, Chio T-H, Yeo T-S. Fabrication of a high-efficiency waveguide antenna array via direct metal laser sintering. *IEEE Antennas and Wireless Propagation Letters*. 2016;**15**: 622-625
- [4] Booth P, Gilmore J, Lluch EV, Harvey M. Enhancements to satellite feed chain performance, testing and lead-times using additive manufacturing. In: 2016 10th European Conference on Antennas and Propagation (EuCAP). 2016. pp. 1-5
- [5] Peverini OA, Lumia M, Calignano F, Addamo G, Lorusso M, Ambrosio EP, et al. Selective laser melting manufacturing of microwave waveguide devices. *Proceedings of the IEEE*. 2017; **105**(4):620-631
- [6] Le Sage GP. 3d printed waveguide slot array antennas. *IEEE Access*. 2016;**4**: 1258-1265
- [7] Silva JS, García-Vigueras M, Debogović T, Costa JR, Fernandes CA, Mosig JR. Stereolithography-based antennas for satellite communications in ka-band. *Proceedings of the IEEE*. 2017; **105**(4):655-667
- [8] Dimitriadis AI, Debogović T, Favre M, Billod M, Barloggio L, Ansermet J-P, et al. Polymer-based additive manufacturing of high-performance waveguide and antenna components. *Proceedings of the IEEE*. 2017;**105**(4):668-676
- [9] Addamo G, Peverini OA, Manfredi D, Calignano F, Paonessa F, Virone G, et al. Additive manufacturing of Ka-band dual-polarization waveguide components. *IEEE Transactions on Microwave Theory and Techniques*. 2018;**66**(8):3589-3596
- [10] Molero C, Legay H, Pierré T, García-Vigueras M. Broadband 3D-printed polarizer based on metallic transverse electro-magnetic unit-cells. *IEEE Transactions on Antennas and Propagation*. June 2022;**70**(6):4632-4644. DOI: 10.1109/TAP.2022.3145435
- [11] Booth P. Additive manufactured bandpass filters at Ka-band. In: 2019 IEEE MTT-S International Microwave Workshop Series on Advanced Materials and Processes for RF and THz Applications (IMWS-AMP). 2019. pp. 7-9
- [12] Polo-López L, Sirici S, Calteau A, Capdevila S, Toso G, Menargues E, et al. Vertically printable evanescent mode filters. *IEEE Microwave and Wireless Components Letters*. 2022. DOI: 10.1109/LMWC.2022.3187781
- [13] An Z, Makdissy T, Vigueras MG, Vaudreuil S, Gillard R. A metal-only reflectarray made of 3d phoenix cells. In: 2022 16th European Conference on Antennas and Propagation (EuCAP). 2022. pp. 1-5
- [14] Charles A, Elkaseer A, Thijs L, Hagenmeyer V, Scholz S. Effect of process parameters on the generated

surface roughness of down-facing surfaces in selective laser melting. *Applied Sciences*. 2019;**9**(6). Article number: 1256. [Online]. Available from: <https://www.mdpi.com/about/announcements/784>

[15] Peverini OA, Addamo G, Lumia M, Virone G, Calignano F, Lorusso M, et al. Additive manufacturing of Ku/K-band waveguide filters: A comparative analysis among selective-laser melting and stereo-lithography. *IET Microwaves, Antennas & Propagation*. 2017;**11**(6): 1936-1942

[16] Sirci S, Menargues E, Billod M. Space-qualified additive manufacturing and its application to active antenna harmonic filters. In: 2021 IEEE MTT-S International Microwave Filter Workshop (IMFW). 2021. pp. 239-242

[17] Sirci S, Menargues E, Berry S. Triangular combline filters conceived for additive manufacturing. In: 2021 IEEE MTT-S International Microwave Filter Workshop (IMFW). 2021. pp. 151-154

[18] Available from: <https://www.eos.info/en/additive-manufacturing/3d-printing-metal/eos-metal-systems/eos-m290>

[19] Available from: <https://www.eos.info/en/additive-manufacturing/3d-printing-metal/eos-metal-systems/eos-m400>

[20] Available from: <https://www.airbus.com/en/newsroom/stories/2021-02-large-scale-3d-printing-goes-to-space-on-airbus-eurostar-neo-satellites>

[21] Available from: <https://swissto12.com/a-large-batch-of-3d-printed-waveguide-solutions-has-been-delivered-to-thales-alenia-space-for-the-eutelsat-konnnect-vhts-program/>

[22] Available from: <https://news.satnews.com/2022/03/16/lockheed-martin-space-partners-with-swissto12-caes-for-advanced-3d-printed-phased-array-antennas/>

[23] Available from: <https://ecss.nl/standard/ecss-q-st-70-80c-processing-and-quality-assurance-requirements-for-metallic-powder-bed-fusion-technologies-for-space-applications-30-july-2021/>

[24] Kähkönen H, Proper S, Ala-Laurinaho J, Viikari V. Comparison of additively manufactured and machined antenna array performance at ka-band. *IEEE Antennas and Wireless Propagation Letters*. 2022;**21**(1):9-13

[25] Tomassoni C, Peverini OA, Venanzoni G, Addamo G, Paonessa F, Virone G. 3D printing of microwave and millimeter-wave filters: Additive manufacturing technologies applied in the development of high-performance filters with novel topologies. *IEEE Microwave Magazine*. 2020;**21**(6):24-45

[26] Wen X, Guo C, Shang X, Yu Y, Shu M, Yang Q, et al. SLM printed waveguide dual-mode filters with reduced sensitivity to fabrication imperfections. *IEEE Microwave and Wireless Components Letters*. 2021; **31**(11):1195-1198

[27] Uher J, Jens B, Uwe R. Artech House Publishers, 1993

[28] Booth P, Skeen M, Stirland S. Low cost, short lead-time feed chain components for multi-beam antennas. In: 2009 3rd European Conference on Antennas and Propagation. 2009, pp. 853-857

[29] Tribak A, Cano JL, Mediavilla A, Boussouis M. Octave bandwidth compact turnstile-based orthomode

transducer. *IEEE Microwave and Wireless Components Letters*. 2010; **20**(10):539-541

[30] Stoumpos C, Fraysse J-P, Goussetis G, Sauleau R, González CG, Pierré T. et al. Four-way orthomode waveguide power dividers: Subtractive and additive manufacturing. In: 2021 15th European Conference on Antennas and Propagation (EuCAP). 2021. pp. 1-5

[31] Stoumpos C, Fraysse J-P, Goussetis G, Sauleau R, Legay H. Quad-furcated profiled horn: The next generation highly efficient GEO antenna in additive manufacturing. *IEEE Open Journal of Antennas and Propagation*. 2022;**3**:69-82

[32] Kilian M, Schinagl-Weiß A, Kohl P, Sommer A, Hartwanger C, Schneider M. Additive layer manufactured waveguide RF components. In: 2019 49th European Microwave Conference (EuMC). 2019. pp. 790-793

[33] Addamo G, Peverini OA, Calignano F, Manfredi D, Paonessa F, Virone G, et al. 3-D printing of high-performance feed horns from Ku- to V-bands. *IEEE Antennas and Wireless Propagation Letters*. 2018;**17**(11):2036-2040

[34] Manafi S, Al-Tarifi M, Filipovic DS. 45–110 GHz quad-ridge horn with stable gain and symmetric beam. *IEEE Transactions on Antennas and Propagation*. 2017;**65**(9):4858-4863

[35] Cailloce Y, Hourlay P, Lebrun F, Palacin B. Additive manufacturing of Ku band horn antennas for telecommunications space applications. In: 12th European Conference on Antennas and Propagation (EuCAP 2018). 2018. pp. 1-4

[36] Huang G-L, Zhou S-G, Sim C-Y-D, Chio T-H, Yuan T. Lightweight

perforated waveguide structure realized by 3-D printing for RF applications. *IEEE Transactions on Antennas and Propagation*. 2017;**65**(8):3897-3904

[37] Veljovic MJ, Skrivervik AK. Circularly polarized axially corrugated feed horn for CubeSat reflectarray applications. In: 2020 14th European Conference on Antennas and Propagation (EuCAP). 2020. pp. 1-4

[38] Foged LJ, Giacomini A, Morbidini R, Saccardi F, Schirosi V, Boumans M, et al. Investigation of additive manufacturing for broadband choked horns at X/Ku band. *IEEE Antennas and Wireless Propagation Letters*. 2018;**17**(11): 2003-2007

[39] Agnihotri I, Sharma SK. Design of a 3D metal printed axial corrugated horn antenna covering full Ka-band. *IEEE Antennas and Wireless Propagation Letters*. 2020;**19**(4):522-526

[40] Fenech H, Sonya A, Tomatis A, Soumphonphakdy V, Merino JLS. Eutelsat Quantum: A Game Changer. [Online]. DOI: 10.2514/6.2015-4318

[41] Elliott R, Kurtz L. The design of small slot arrays. *IEEE Transactions on Antennas and Propagation*. 1978;**26**(2): 214-219

[42] Tyagi Y, Mevada P, Chakrabarty S, Mahajan M. Broadband slotted waveguide array antenna with novel impedance matching network. In 2019 IEEE Indian Conference on Antennas and Propagation (InCAP). 2019. pp. 1-5

[43] Wang W, Zhong S-S, Zhang Y-M, Liang X-L. A broadband slotted ridge waveguide antenna array. *IEEE Transactions on Antennas and Propagation*. 2006;**54**(8):2416-2420

- [44] Zhao H, Xu R, Wu W. Broadband waveguide slot array for SAR. *Electronics Letters*. 2011;**47**(02):76-77
- [45] Tyagi Y, Mevada P, Chakrabarty S, Jyoti R. High efficiency broadband slotted waveguide array antenna. *IET Microwaves, Antennas & Propagation*. 2017;**11**:05
- [46] Huang G-L, Zhou S-G, Chio T-H. Highly-efficient self-compact monopulse antenna system with integrated comparator network for RF industrial applications. *IEEE Transactions on Industrial Electronics*. 2017;**64**(1): 674-681
- [47] Martin-Guennou A, Quéré Y, Rius E, Person C, Enouz-Vedrenne S, Lesueur G, et al. Direct metal laser sintering process investigation: Application to 3D slotted waveguide antennas. *IET Microwaves, Antennas & Propagation*. 2007;**11**(14): 1921-1929
- [48] Oliner AA. In: Johnson RC, editor. *Antenna Engineering Handbook*. 3rd ed. New York: McGraw-Hill; 1993
- [49] García-Vigueras M. Cost-effective dual-polarised leaky-wave antennas enabled by three-dimensional printing. *IET Microwaves, Antennas Propagation*. 2017;**11**(6):1985-1991
- [50] Dorlé A, Gillard R, Menargues E, der Vorst MV, de Rijk E, Martín-Iglesias P et al. Sidelobe level reduction in ridged leaky waveguide through stereolithography. In: 2019 13th European Conference on Antennas and Propagation (EuCAP). 2019. pp. 1-5
- [51] Dorlé A, Gillard R, Menargues E, Van Der Vorst M, De Rijk E, Martín-Iglesias P, et al. Additive manufacturing of modulated triple-ridge leaky-wave antenna. *IEEE Antennas and Wireless Propagation Letters*. 2018;**17**(11): 2123-2127
- [52] Dorlé A, Gillard R, Menargues E, Van Der Vorst M, De Rijk E, Martín-Iglesias P, et al. Circularly polarized leaky-wave antenna based on a dual-mode hollow waveguide. *IEEE Transactions on Antennas and Propagation*. 2021;**69**(9):6010-6015
- [53] Munk B. *Frequency Selective Surfaces: Theory and Design*. Melville, NY, USA: Wiley; 2005. Available from: <https://aip.scitation.org/jap/info/contact>
- [54] Ehrenberg IM, Sarma SE, Wu B-I. A three-dimensional self-supporting low loss microwave lens with a negative refractive index. *Journal of Applied Physics*. 2012;**112**(7):073114
- [55] Chen B-J, Yi H, Ng KB, Qu S-W, Chan, CH. 3D printed reflectarray antenna at 60 GHz. In: 2016 International Symposium on Antennas and Propagation (ISAP). 2016. pp. 92-93
- [56] Velasco J, Parellada-Serrano I, Molero C. Fully metallic reflectarray for the Ku-band based on a 3D architecture. *Electronics*. 2021;**10**(21)
- [57] Tang W, Zhu J, Wang C, Ge J, Yu Z, and Zhuang W. Waveguide 3-D FSSs by 3-D printing technique. In: 2016 International Conference on Electromagnetics in Advanced Applications (ICEAA). 2016. pp. 675-678
- [58] Kien N, Hong I-P. Application of metaheuristic optimization algorithm and 3D printing technique in 3D bandpass frequency selective structure. *Journal of Electrical Engineering & Technology*. 2020;**15**:02
- [59] Fernández Álvarez H, Cadman D, Goulas A, Gómez M, Engstrom D,

Vardaxoglou J, et al. 3D conformal bandpass millimeter-wave frequency selective surface with improved fields of view. *Scientific Reports*. 2021;**11**:06

[60] Wu S, Yachin VV, Shcherbinin VI, Tuz VR. Chiral metasurfaces formed by 3D-printed square helices: A flexible tool to manipulate wave polarization. *Journal of Applied Physics*. 2019;**126**(10):103101

[61] Wu G-B, Zeng Y-S, Chan KF, Qu S-W, Chan CH. 3-D printed circularly polarized modified fresnel lens operating at terahertz frequencies. *IEEE Transactions on Antennas and Propagation*. 2019;**67**(7):4429-4437

[62] Wang X, Cheng Y, Dong Y. Millimeter-wave dual-polarized metal transmitarray antenna with wide gain bandwidth. *IEEE Antennas and Wireless Propagation Letters*. 2022;**21**(2):381-385

[63] Molero C, Menargues E, Garcia-Vigueras M. All-metal 3-D frequency-selective surface with versatile dual-band polarization conversion. *IEEE Transactions on Antennas and Propagation*. 2020;(02): 1-1

[64] Bermúdez D, Molero C, Legay H, Palacin B, Menargues E, Gillard R, et al. Synthesis of versatile functionalities in arrangements of 3D unit-cells. In: 2021 IEEE Conference on Antenna Measurements Applications (CAMA). 2021. pp. 372-376